Physics of the Earth and Planetary Interiors 251 (2016) 1–10

Contents lists available at ScienceDirect

Physics of the Earth and Planetary Interiors

journal homepage: www.elsevier.com/locate/pepi

Effect of post-perovskite rheology on the thermal evolution of the Earth

Nina Benešová *, Hana Čížková

Department of Geophysics, Faculty of Mathematics and Physics, Charles University, V Holešovičkách 2, 180 00 Prague 8, Czech Republic

ARTICLE INFO

Article history:
Received 21 January 2015
Received in revised form 25 October 2015
Accepted 17 November 2015
Available online 8 December 2015

Keywords:
Post-perovskite
Earth evolution
Mantle convection
Phase transitions

ABSTRACT

Secular cooling of the Earth mantle is a complex process affected by many factors. Here we present the results of a modelling study focused on efficiency of cooling in the presence of rheologically distinct post-perovskite. We evaluate combined effects of variable thermal expansivity and diffusivity, initial thermal condition and heat source model and concentrate on the effects of rheologically weak post-perovskite. Cooling of the core is included in the model—core is assumed to be an isothermal heat reservoir with temperature controlled by heat flux through core–mantle boundary. Our 2D axisymmetric convection model has pressure, temperature and phase dependent viscosity and includes the effects of an endothermic phase transition at 660 km depth and an exothermic perovskite-post-perovskite phase transition in the lowermost mantle. In agreement with previous studies we conclude that depth-dependent material parameters tend to delay secular cooling. Presence of the weak post-perovskite on the other hand significantly enhances core cooling and its effect on core temperature is opposite and comparable in magnitude.

1. Introduction

Thermal evolution of the Earth mantle has been addressed in past decades in terms of volume averaged or parameterised models and recently also in fully dynamical simulations of convection. Numerous studies focused on various phenomena that affect cooling of the Earth mantle (e.g. Breuer and Spohn, 1993; Honda and Iwase, 1996; DeLandro-Clarke and Jarvis, 1997; van den Berg and Yuen, 2002; Butler and Peltier, 2002; Nakagawa and Tackley, 2004a, 2005a; van den Berg et al., 2004; Korenaga, 2006; Labrosse and Jaupart, 2007; Korenaga, 2010) and through the core–mantle coupling also the core evolution and magnetic field generation.

A new phenomenon that could potentially influence core–mantle coupling and cooling of the Earth appeared in 2004. Discovery of post-perovskite (PPV) (Murakami et al., 2004; Oganov and Ono, 2004) motivated many studies that investigated its effects on the mantle convection. This exothermic phase transition has high Clapeyron slope—its value was estimated between 8 MPa/K (Tsuchiya et al., 2004) and 13 MPa/K (Tateno et al., 2009)—but a small density contrast of 1%. High Clapeyron slope results in strongly variable depth of the PPV transition and, with higher core–mantle boundary (CMB) temperatures, double-crossing of this phase boundary occurs and isolated lenses of PPV are formed (Nakagawa and Tackley, 2005b; Monnereau and Yuen, 2007). Density anomalies associated with the exothermic phase change tend to enhance convective vigour and increase number of plumes (Nakagawa and Tackley, 2004b, 2006; Matyska and Yuen, 2005) though this effect is not particularly strong due to small density contrast. Presence of PPV could however enhance the effects of other parameters, such as strongly variable thermal conductivity (Matyska and Yuen, 2006). PPV phase transition was further found to destabilize chemically-dense material piling above the CMB and allow penetration of cold slabs into dense material (Nakagawa and Tackley, 2005b), though this destabilising effect is less if the PPV transition depends on composition and occurs at lower pressure in chemically-dense material. Finally, PPV transition was found to increase CMB heat flux (Nakagawa and Tackley, 2004b, 2008).

Moderate effects of the lowermost mantle phase transition on convection may be further enhanced if we take into account different transport properties of PPV, especially its viscosity. Despite the fact that rheology of PPV is still not sufficiently well described, there are some indications that it may be (possibly significantly) weaker than perovskite either through dislocation creep viscosity (Carrez et al., 2007) or due to a considerably lower diffusion creep viscosity (Ammann et al., 2010). Another possible mechanism that could produce PPV weaker than perovskite at the same pressure and temperature conditions could be grain size reduction associated with the phase transition (Karato et al., 2001; Solomatov and Moresi, 2002). On the other hand, the viscosity of PPV is highly

* Corresponding author.
E-mail address: benesova@karel.troja.mff.cuni.cz (N. Benešová).

http://dx.doi.org/10.1016/j.pepi.2015.11.004
0031-9201/

anisotropic and it has been argued (Karato, 2010) that currently available knowledge is insufficient to constraint the viscosity, and based on the calculations, it can actually be comparable or even higher than that of the perovskite. An independent constraint on the PPV viscosity could be provided by geoid inversion. Long-wavelength geoid is highly sensitive to the presence of low viscosity areas located in the subducted slabs at the base of the mantle (Tosi et al., 2009) and it has been shown by Čadek and Fleitout (2006) that the results of geoid inversion suggest low viscosity in the paleoslab areas in D″ layer, where PPV should be present thanks to relatively low temperatures.

Rheologically weak PPV may considerably affect dynamics of cold downwelling slabs, further enhance lowermost mantle convective velocities and CMB heat flux (Čížková et al., 2010; Nakagawa and Tackley, 2011; Li et al., 2014) and increase mantle temperatures and mixing efficiency (Tosi et al., 2010; Samuel and Tosi, 2012). Weak PPV has been reported to slightly decrease the stability and increase the topography and steepness of dense reservoirs, nevertheless those reservoirs remain stable during the period comparable to the age of the Earth (Li et al., 2014). It also produces seismic velocity anomalies consistent with observations (van den Berg et al., 2010) and affects geoid above slabs through enhancement of flow in the lowermost mantle (Tosi et al., 2009). Furthermore, Amit and Choblet (2009) concluded that if the effect of PPV on enhancing CMB heat flux is taken into account, consistency of geodynamo models with the observations is improved.

In the early Earth, mantle was probably too hot to allow for the PPV formation. During mantle cooling PPV appeared at certain moment and may have exerted potentially strong effects on mantle evolution by increasing core–mantle heat flux and thus enhancing core cooling. Some of these effects have already been discussed also in terms of long-term models. Model of mantle thermal evolution and associated core cooling and inner-core growth of Nakagawa and Tackley (2010) included PPV phase transition, but did not take into account low viscosity PPV. They report weak dependence of the system on the initial CMB temperature and strong dependence on the chemical contrast in the deep mantle. Dense piles accumulated at the CMB facilitate obtaining correct final inner core size and maintaining geodynamo. Weak sensitivity to initial CMB temperature was confirmed in Nakagawa and Tackley (2012a), where magmatism was identified as dominant mechanism of heat loss in early stages of Earth evolution. Finally, Nakagawa and Tackley (2011) concentrated on the effect of weak PPV and concluded that it increases lateral extent of chemical anomalies and reduces CMB topography by weakening the slabs at the base of the mantle. As already pointed out before, it also increases CMB heat flux and should therefore potentially influence the rate of core cooling. Core cooling was however not included in their model.

Here we supplement these previous studies by investigating effects of rheologically distinct post-perovskite on the mantle cooling in the model that includes decaying heat sources and heat extraction from the core. Core is assumed to be an isothermal heat reservoir with temperature controlled by heat flux through CMB. We simulate long-term evolution of the mantle from hot initial state and we evaluate combined effects of weak post-perovskite and several other parameters (thermal expansivity, diffusivity, initial core temperature).

2. Model description

Thermal convection in the mantle is described by the set of equations including the conservation of mass, momentum and energy and further by the constitutive equation and the equation of state. These equations together with the initial and boundary conditions describe the motion of the fluid driven by thermal buoyancy. For incompressible Newtonian fluid in extended Boussinesq approximation we have the following set of equations:

$$\nabla \cdot \mathbf{v} = 0, \tag{1}$$

$$\nabla \cdot \tau + \varrho \mathbf{g} = 0, \tag{2}$$

$$\varrho_0 c_p \frac{\partial T}{\partial t} = \nabla \cdot (k \nabla T) - \varrho_0 c_p \mathbf{v} \cdot \nabla T - \varrho_0 v_r \alpha T g + \sigma : \nabla \mathbf{v} + H + L_t, \tag{3}$$

$$\tau = -pI + \eta(\nabla \mathbf{v} + \nabla^T \mathbf{v}), \tag{4}$$

where $\mathbf{v}$ is the flow velocity, τ is the stress tensor, σ is the deviatoric part of the stress tensor, ϱ is the density, $\mathbf{g}$ is the gravity acceleration, t is the time, v_r is the radial component of velocity, c_p is the specific heat at constant pressure, T is the temperature, k is the thermal conductivity, ϱ_0 is the reference density, α is the thermal expansivity, H denotes volume heat sources, p is the pressure, I is the identity matrix, η is the viscosity and L_t is the latent heat. The density depends linearly on temperature

$$\varrho = \varrho_0[1 - \alpha(T - T_0)], \tag{5}$$

where T_0 is the reference temperature corresponding to the reference density ϱ_0.

We solve the set of Eqs. (1)–(5) in a 2D axisymmetric domain bounded by the core–mantle boundary at the bottom and the surface at the top. On both of them we prescribe impermeable free-slip boundary conditions. Constant temperatures T_{top} and T_{cmb} are prescribed on the top and bottom surfaces, respectively.

We use two models of internal heating rate and its time decay. Model H1 assumes equation

$$H(t) = \sum_{i=U,Th,K} H_0^i \exp\left(-\frac{t \ln 2}{\tau^i}\right), \tag{6}$$

where initial productions of individual radioactive elements H_0^i are calculated from their present-day values and half-lives τ^i (Lowrie, 2007), see Table 1. As the proportion of ^{235}U in natural uranium is about 0.71% while that of ^{238}U is 99.28%, the effect of ^{235}U is omitted here. It may be potentially more important in the early Earth due to its relatively short half-life (0.704 Ga) but still its contribution to total internal heating budget was about 5 TW and rapidly decreasing.

Second model of internal heating H2 follows relation

$$H(t) = \frac{1}{M}((10.26t + 51.16)\exp(-t) - 2.49t + 26.78), \tag{7}$$

where $M = 3.63216 \cdot 10^{24}$ kg is the mass of the Earth. This formula was interpolated from van Schmus (1995). Time evolution of internal heating rate in both models is illustrated in Fig. 1a.

Viscosity depends on pressure (through radius r) and temperature following formula

$$\eta(r, T) = \Delta\eta_l \Delta\eta_{660} \Delta\eta_{ppv} \eta_0 \exp\left[a\frac{r_{top} - r}{r_{top} - r_{cmb}} - b\frac{T - T_{top}}{T_{cmb} - T_{top}}\right]. \tag{8}$$

An arbitrarily chosen parameter η_0 controls Rayleigh number, $a = 4.6052$ results in two orders of magnitude viscosity increase

Table 1
Values of half-lives and heating rates for internal heating model H1.

Element	τ^i [Ga]	H(4.5 Ga)	H_0^i [W/m^3]
Uranium	4.5	$9.52 \cdot 10^{-9}$	$19.2 \cdot 10^{-9}$
Thorium	14	$8.92 \cdot 10^{-9}$	$11.2 \cdot 10^{-9}$
Potassium	1.3	$0.96 \cdot 10^{-9}$	$11.6 \cdot 10^{-9}$

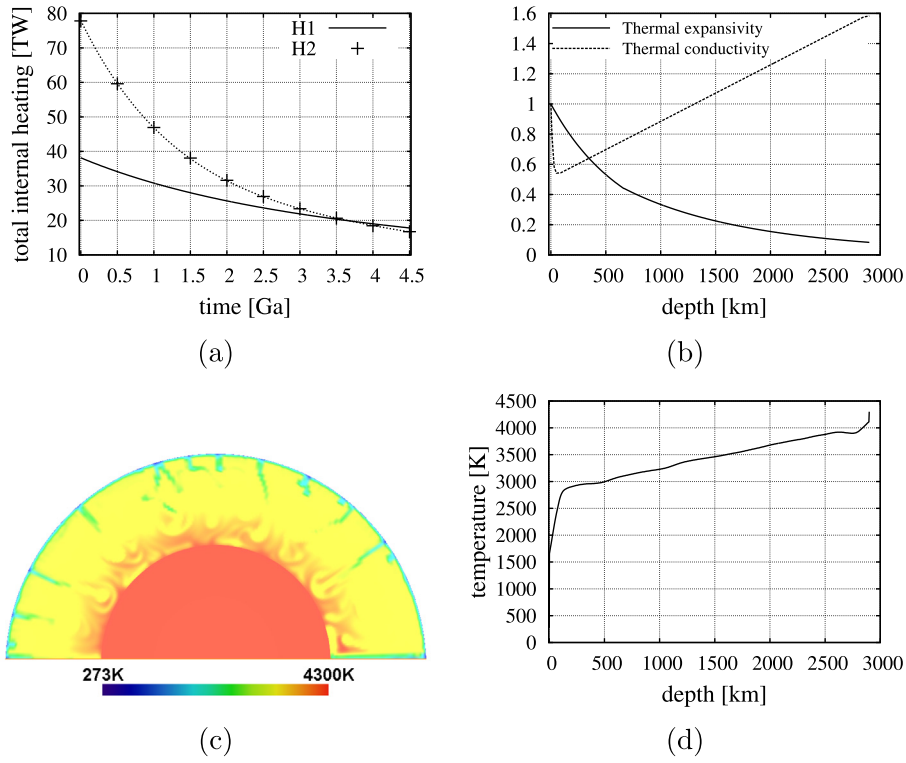

Fig. 1. (a) two models of internal heating used in this study, (b) thermal conductivity and expansivity scaled by surface value, (c) initial temperature distribution and (d) average geotherm of initial temperature distribution.

with depth while $b = 5.0106$ determines temperature variations of viscosity of the order of 150. As this temperature dependence is relatively weak we apply additional viscosity contrast $\Delta\eta_l$ which is depth dependent. In uppermost 100 km of the model $\Delta\eta_l = 10$ to produce stronger lithosphere. In the rest of the mantle $\Delta\eta_l = 1$. Additional viscosity variations ($\Delta\eta_{660}, \Delta\eta_{ppv}$) are introduced due to phase transitions (see below).

Thermal conductivity is either constant k_0 or radially-dependent. The model of radially dependent $k(r)$ (Fig. 1b) based on pressure and temperature dependent model of Hofmeister (1999) is taken from van den Berg et al. (2005). The surface value of radially dependent conductivity is $k_{top} = 4.8\ \mathrm{W\,m^{-1}\,K^{-1}}$. Thermal expansivity is either constant α_0 or radially dependent (Matyska et al., 2011) with surface value α_0:

$$\begin{aligned} \tfrac{\alpha}{\alpha_0} &= (1 + 0.78z)^{-5} && \text{if } 0 \leqslant z \leqslant 0.23, \\ \tfrac{\alpha}{\alpha_0} &= 0.44(1 + 0.35(z - 0.23))^{-7} && \text{if } 0.23 \leqslant z \leqslant 1, \end{aligned} \tag{9}$$

where z is non-dimensional depth. Dimensionless values of both parameters are given in Fig. 1b.

Heat extracted from the core during long-term cooling should be reflected in decreasing CMB temperature T_{cmb}. In our model the core is considered to be an isothermal heat reservoir and its temperature T_C is controlled by the total heat flux through core–mantle boundary Q_{cmb} (van den Berg et al., 2005):

$$\frac{\mathrm{d}T_C}{\mathrm{d}t} = -\frac{Q_{cmb}(t)}{\varrho_C c_{pC} V_C}. \tag{10}$$

Here ϱ_C is the density of the core, c_{pC} is the specific heat of the core at constant pressure and V_C is the volume of the core. The term $\varrho_C c_{pC} V_C$ is the total heat capacity of the core. This equation is solved together with the thermal equation and at each time step the new core temperature is evaluated and the boundary condition is updated so that $T_{cmb} = T_C$.

All models include the spinel-perovskite endothermic phase transition at 660 km depth (for parameters see Table 2). In some models, perovskite to PPV exothermic transition is prescribed with moderate Clapeyron slope of 10 MPa/K, density contrast of 1% and temperature intercept $T_{int} = 3800$ K (the temperature of the PPV transition at the CMB pressure). Both phase transitions are parametrised with a harmonic phase function Γ (van Hunen et al., 2004). Transition width of 660 km phase transition is 40 km, while for the PPV transition we assume relatively broad transition width of 200 km to facilitate numerical stability of the model runs. Such a wide transition is however supported by in situ experiments of Catalli et al. (2009). In the models where perovskite to PPV

Table 2
Model parameters.

Parameter	Symbol	Value	Units
radius of the Earth	r_{top}	6371	km
core radius	r_{cmb}	3471	km
gravity acceleration	g	9.87	$\mathrm{m\,s^{-2}}$
reference density	ρ_0	4000	$\mathrm{kg\,m^{-3}}$
specific heat at constant pressure	c_p	1250	$\mathrm{J\,kg^{-1}\,K^{-1}}$
thermal expansivity (surface value)	α_0	$2.5 \cdot 10^{-5}$	$\mathrm{K^{-1}}$
thermal conductivity	k_0	5.9	$\mathrm{W\,m^{-1}\,K^{-1}}$
density of the core	ϱ_C	12500	$\mathrm{kg\,m^{-3}}$
specific heat of the core	c_{pC}	500	$\mathrm{J\,kg^{-1}\,K^{-1}}$
temperature on the surface	T_{top}	273	K
Clapeyron slope (660 km)	γ_{660}	−2.5	$\mathrm{MPa\,K^{-1}}$
density jump (660 km)	$\delta\rho_{660}$	342	$\mathrm{kg\,m^{-3}}$
temperature of 660 km phase transition	T_{660}	1800	K
width of the 660 km transition	d^{ph}_{660}	40	km
viscosity jump at 660 km	$\Delta\eta_{660}$	10	
Clapeyron slope of PPV phase transition	γ_{ppv}	10	$\mathrm{MPa\,K^{-1}}$
density jump at PPV phase transition	$\Delta\rho_{ppv}$	40	$\mathrm{kg\,m^{-3}}$
temperature intercept	T_{int}	3800	K
width of PPV phase transition	d^{ph}_{ppv}	200	km
viscosity reduction of PPV	$\Delta\eta_{ppv}$	1, 0.1, 0.01, 0.001	

transition is assumed, PPV phase is always weaker than perovskite – by one to three orders of magnitude at the same pressure and temperature conditions. In these model cases parameter $\Delta\eta_{ppv}$ in formula (8) is 0.1, 0.01 or 0.001 within the PPV stability area, otherwise $\Delta\eta_{ppv} = 1$. In models referenced as "without PPV" neither effect of the phase transition is considered (viscosity, density or latent heat). Phase transition at 660 km depth is associated with the viscosity increase by a factor of 10 ($\Delta\eta_{660} = 1$ in the upper mantle, $\Delta\eta_{660} = 10$ throughout the lower mantle) and density increase of 342 kg m^{-3}.

The viscosity contrast between the lithosphere and the underlying mantle is rather small compared to what one would expect for the Earth. As the treatment of realistic lithosphere rheology and associated complex plate deformations is beyond the reach of the code we use somewhat lower lithospheric viscosity that produces mobile lid. We also assume rather small thermal viscosity contrast.

Parameters used in our study are summarised in Table 2.

The style of convection depends on the mantle material parameters, density ϱ, thermal expansivity α, diffusivity κ and viscosity η as well as the shell thickness d. Their joint influence can be characterised by a single dimensionless parameter – the Rayleigh number:

$$Ra = \frac{\varrho\alpha g(T_{cmb} - T_{top})d^3}{\kappa\eta}. \quad (11)$$

In the models with spatially variable parameters, Ra depends on the choice of the reference values of the parameters in (11). Viscosity varies by more than 2 orders of magnitude throughout the model domain which definitely makes the choice of its reference value difficult. Further, in some models thermal expansivity decreases by a factor of 5 and thermal conductivity also varies with depth. We will therefore use here the Rayleigh number of "well-mixed interior" – we will calculate Ra according to (11) using parameter values at 500 km depth.

We performed series of 2D axisymmetric model runs with initial $Ra = 2.6 \times 10^7$ (we refer to them as P-10^7) and 1.6×10^8 (P-10^8) and varying parameters. All model runs are summarised in Table 3.

To solve the set of Eqs. (1)–(5) we apply a semi-spectral method (Benešová and Čížková, 2012). Both radial and lateral resolution varies among individual models. Typical radial resolution of lower $Ra(10^7)$ calculations is 20 km and cut-off degree is 250, higher $Ra(10^8)$ models have radial resolution 5 km and cut-off degree 550.

Initial distribution of temperature should represent overheated early Earth. Following van den Berg et al. (2005) we obtained this initial temperature from a statistical steady-state solution of a model run with extremely high internal heating rate (approximately ten times higher then present day value - $\sim 4.7 \cdot 10^{-11}$ W/kg) with thermal bottom boundary condition constant in time $T_{cmb} = 4300$ K. Rayleigh number of this initial run was $Ra = 10^8$ and viscosity was constant. All other parameters were the same as in regular model runs (see Table 2).

Table 3
List of presented models. Column 'ppv' indicates whether there is post-perovskite phase transition or not—1 means ppv is 1 order weaker (viscosity) than perovskite, similarly 2 and 3 orders, $Ra^{t=0}$ and $T^{t=0}_{cmb}$ are values at the beginning of the calculation, H indicates the type of internal heating, column k indicates thermal conductivity ($k(r)$ denotes radial profile) and column α indicates constant or radially dependent thermal expansivity.

model name	ppv	$Ra^{t=0}$	H	$T^{t=0}_{cmb}$ [K]	k [W/mK]	α [K^{-1}]
P0-$10^7$4300H1	no	2.6×10^7	H1	4300	5.9	$2 \cdot 10^{-5}$
P1-$10^7$4300H1	1					
P2-$10^7$4300H1	2					
P3-$10^7$4300H1	3					
P0-$10^7$4500H1	no			4500		
P2-$10^7$4500H1	2					
P0-$10^7$6000H1	no			6000		
P2-$10^7$6000H1	2					
P0-10^7k4300H1	no			4300	$k(r)$	
P2-10^7k4300H1	2					
P0-$10^7$4300H2	no		H2		5.9	
P2-$10^7$4300H2	2					
P0-$10^7\alpha$4300H2	no					$\alpha(r)$
P2-$10^7\alpha$4300H2	2					
P0-10^7kα4300H2	no				$k(r)$	
P2-10^7kα4300H2	2					
P0-10^7kα4500H2	no			4500		
P2-10^7kα4500H2	2					
P0-10^7kα6000H2	no			6000		
P2-10^7kα6000H2	2					
P0-10^8kα4500H2	no	1.6×10^8		4500		
P2-10^8kα4500H2	2					

3. Results and discussion

First let us discuss the results of models with lower initial $Ra = 10^7$ with constant expansivity and diffusivity. Cooling of the Earth in reference model without weak PPV is shown in Fig. 2a. Here time evolution of temperature is plotted in four snapshots. In the first snapshot (1.5 Ga) mantle is hot with four plumes rising from the CMB region. Some of the cold downwellings are hindered at the 660 km boundary due to the combined effects of endothermic phase transition and viscosity increase. Both mantle and core are cooling with time, tendency to layered flow pattern is decreasing and in the final snapshot most downwellings reach lower mantle, though some of them are temporarily deflected at 660 km interface. (The only exception is polar region where plume-slab interaction occurs. This is however an anomalous position where vertical cylindrical features are enforced by axisymmetric geometry.) The lifetime of observed downwellings is variable, but the duration of some of them is up to 1 Ga. The evolution of core temperature is demonstrated in Fig. 3a (red curve). Core cooling is inefficient in the first 0.5 Ga, due to the low plume activity. At the beginning, large volumetric heating is damping the development of thermal instabilities in the bottom thermal boundary layer. Plumes are less vigorous, and heat transfer is dominated by downwellings. This effect is well documented in various geometry (e.g. Travis and Olson, 1994; Sotin and Labrosse, 1999; Deschamps et al., 2010). When radiogenic heating is low enough (below ~35 TW, at around 0.5 GYr in case of the model P0-10^7 4300H1), plumes become more vigorous and can extract heat from the core and bring it to the surface. Core heat flux is thus decreasing in the initial 0.5 Ga (Fig. 3b) and very short periods of negative heat flux may even appear when core is temporarily warming. After this initial period, CMB heat flux increases and core temperature is decreasing steadily. The evolution of viscosity in the same model run is plotted in Fig. 2d. As expected, viscosity is increasing with time during mantle cooling.

If PPV weaker by two orders of magnitude is taken into account we observe some changes in character of flow (Fig. 2b). PPV first appears in the coldest material above CMB at about 0.5 Ga after the initial state. In the first snapshot of Fig. 2e (1.5 Ga) reduced viscosity of PPV is visible in both massive polar downwellings. Weakening of the cold foot of the slab results in enhanced lateral flow

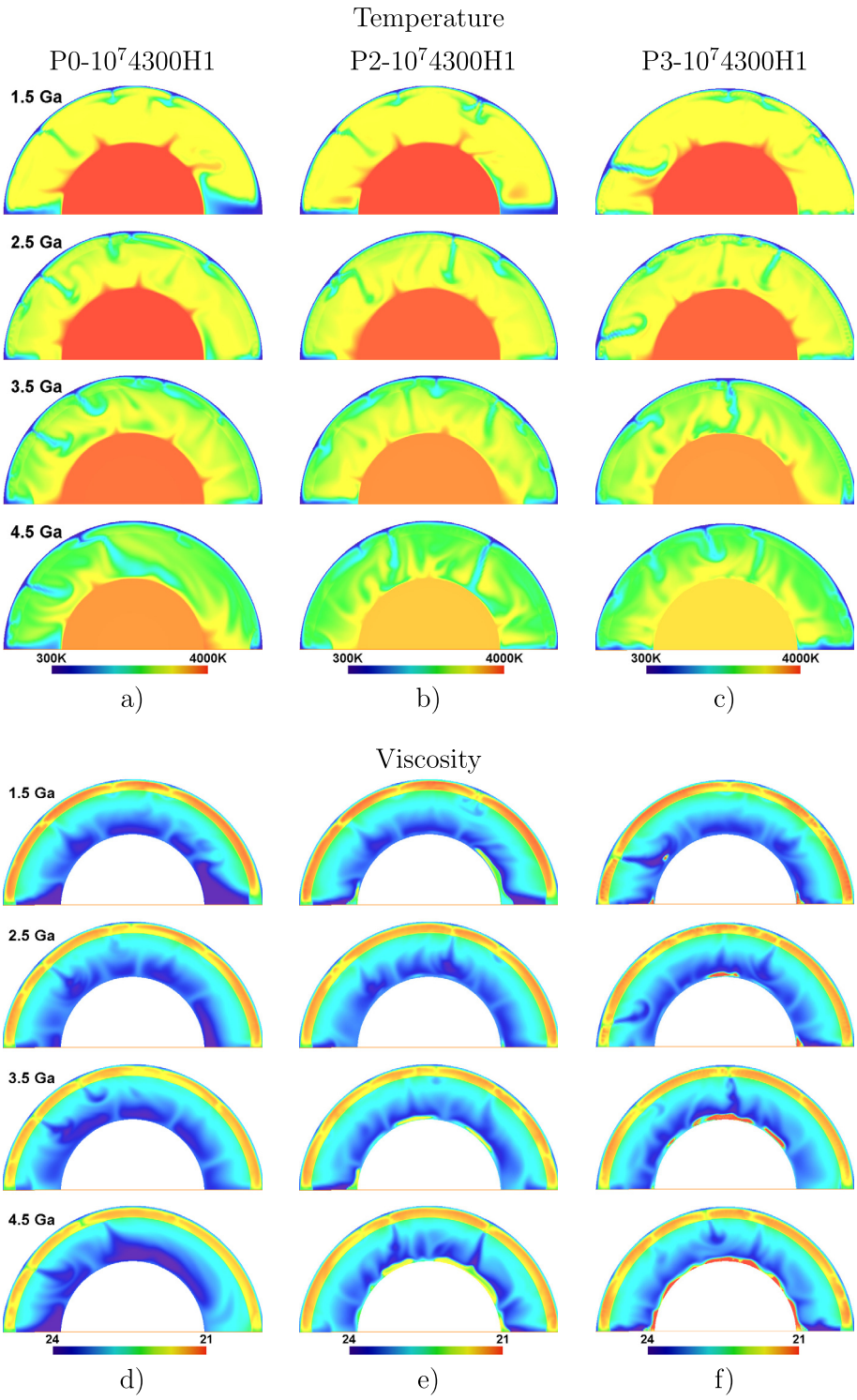

Fig. 2. Models P-$10^7$4300H1: time evolution of temperature and viscosity (in log-scale).

above the CMB and consequently the downwellings are thinner than in case without bottom weakening (cf. Fig. 2a and b, first snapshot). Higher mobility of cold material in the bottom boundary layer increases CMB heat flux (Fig. 3b, blue curve) and makes core cooling more efficient (Fig. 3a, blue curve). Resulting core temperature is thus by 180 K lower than in model without weak PPV. Yet lower PPV viscosity (PPV weaker by three orders of magnitude—model P3-$10^7$4300H1, Fig. 2cf) further enhances CMB heat flux, especially in the time intervals when massive cold downwellings arrive at the CMB. Resulting CMB temperature is thus by about 80 K lower than in case of PPV viscosity reduction by two orders of magnitude (Fig. 3a, purple curve).

Rheologically weak PPV reduces core temperature, but does not strongly affect average mantle temperature in upper two thirds of the mantle. Geotherms only differ in bottom 1000 km by up to 250 K. These temperature differences affect horizontally averaged viscosity (Fig. 4a) and together with PPV viscosity reduction are thus responsible for different core cooling efficiency.

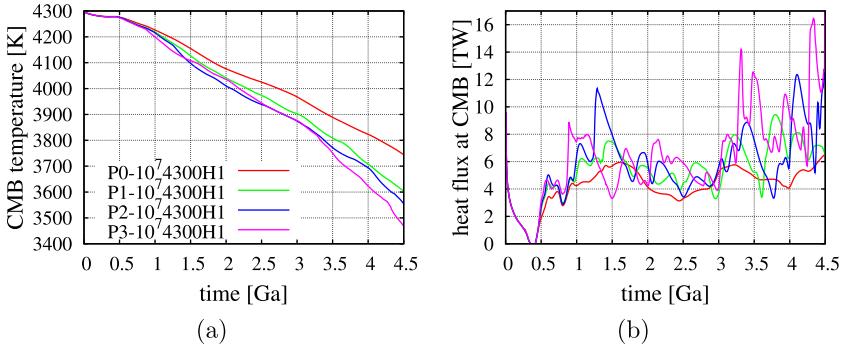

Fig. 3. Models P-$10^7$4300H1: time evolution of core–mantle boundary temperature, and heat flux at the core–mantle boundary.

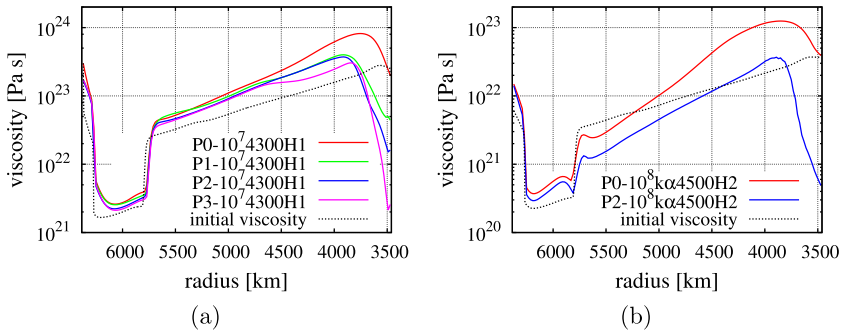

Fig. 4. Models P-$10^7$4300H1 and P-$10^8$4500H2: horizontally averaged viscosity. Black dotted line is at $t = 0$ (initial condition), red, green and blue lines are taken at 4.5 Ga. (For interpretation of the references to color in this figure legend, the reader is referred to the web version of this article.)

In addition to PPV viscosity, there are apparently some other model parameters that affect cooling efficiency. Fig. 5 summarizes effects of some of them, namely initial core temperature, depth-dependent thermal conductivity, internal heating rate, depth-dependent thermal expansivity and combination of these. For each model final snapshot of temperature is shown. First let us look at the effect of depth-dependent conductivity (Fig. 5a). Here relatively low conductivity at shallow depths suppresses heat extraction from the mantle and results in significantly higher mantle temperatures. Warmer mantle is in turn less efficient in extracting heat from the core and the final CMB temperature is thus by about 100 K higher than in the reference case (cf. black line in Fig. 6a). Thermal expansivity decreasing with depth (Fig. 5b) results in long-wavelength lower-mantle downwellings and sluggish convection that is significantly less efficient in removing heat from the core. CMB temperature (Fig. 6a, green curve) is thus higher than in reference model. Furthermore, note that effect of an endothermic phase transition at 660 km is more pronounced in models with decreasing expansivity. Here the thermal buoyancy of both upwelling and downwelling features at 660 km depth is more than twice lower than in constant expansivity case, while the negative buoyancy associated with the phase transition is the same (controlled by the same Clapeyron slope). Higher initial internal heating rate (P0-$10^7$4300H2, Fig. 5c) produces final state with average mantle temperature slightly higher than in reference case (Fig. 6a, cf blue and black curves) thanks to the fact that cooling rate in the initial 1 Ga is much less efficient than in reference case. Combination of depth-dependent expansivity and conductivity is further studied in model presented in Fig. 5d. Both parameters tend to stabilize lower-mantle circulation and result in relatively slow long-wavelength flow and consequently in significantly warmer mantle and core. Endothermic phase transition at 660 km depth acts as a more effective barrier in these models and we observe partially layered convection that is so inefficient in removing heat from the lower mantle, that average mantle temperature is increasing within first 1.5 Ga of mantle evolution (Fig. 6a, magenta curve).

Finally, let us discuss the models with higher initial CMB temperatures – 4,500 K and 6,000 K. Model with very high initial CMB temperature and constant parameters (Fig. 5e) results in similar flow pattern as reference model P0-$10^7$4300H1 (Fig. 2a, last panel), though the average mantle temperature is significantly higher than in reference case. Similarly, model with high initial CMB temperature and variable conductivity and expansivity (Fig. 5f), is also significantly warmer but otherwise shows similar characteristic features as corresponding model with lower CMB temperature (Fig. 5d). Models with higher initial temperature result in warmer state, their cooling is however more efficient – CMB temperature drop over the model calculation is almost twice higher in models with initial CMB temperature of 6,000 K (cf. Fig. 6b).

The effect of weak PPV in models with variable parameters (Fig. 5g–l) is similar to the above discussed PPV effect in model with constant properties (Fig. 2). In all models weak PPV results in higher mobility of the lowermost mantle and in enhanced cooling efficiency. Models with weak PPV thus result in lower CMB temperature than their counterparts without PPV (Fig. 6, cf solid and dotted lines).

Finally, we will evaluate the effects of higher initial $Ra = 10^8$. We will use the model with combined effects of depth-dependent parameters $k(r)$ and $\alpha(r)$ and initial CMB temperature of 4500 K. Temperature in the last snapshot of simulation is shown in Fig. 7, panel (a) is for model without weak PPV, panel (b) for model with PPV by two orders of magnitude weaker than perovskite. Weak PPV in combination with depth-dependent properties clearly have much stronger effect in this more vigorous convection model with depth-dependent parameters. Endothermic phase transition at 660 km associated with viscosity increase now

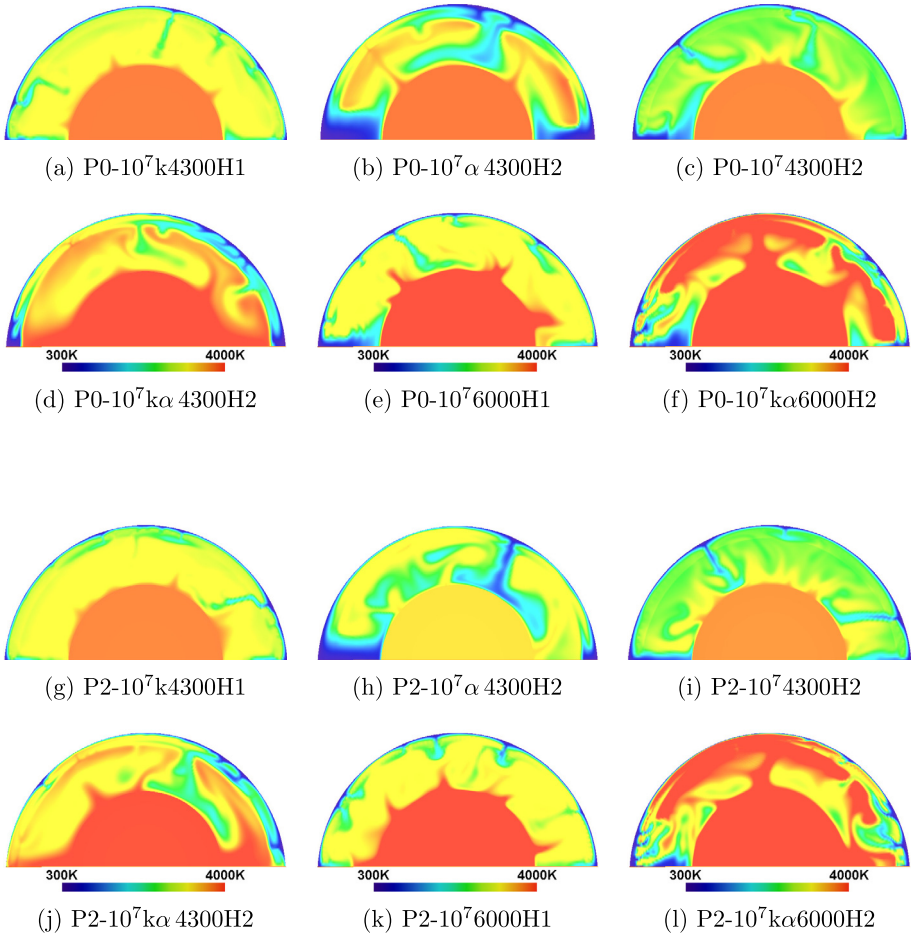

(a) P0-10^7k4300H1 (b) P0-$10^7\alpha$ 4300H2 (c) P0-$10^7$4300H2

(d) P0-10^7kα 4300H2 (e) P0-$10^7$6000H1 (f) P0-10^7kα6000H2

(g) P2-10^7k4300H1 (h) P2-$10^7\alpha$ 4300H2 (i) P2-$10^7$4300H2

(j) P2-10^7kα 4300H2 (k) P2-$10^7$6000H1 (l) P2-10^7kα6000H2

Fig. 5. Snapshot of temperature taken at 4.5 Ga for models P0-10^7 and P2-10^7.

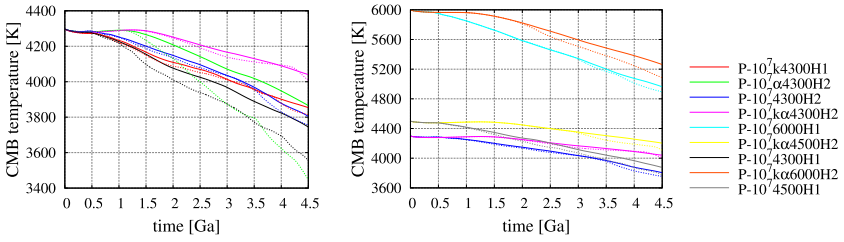

(a) (b)

Fig. 6. Models P-10^7: time evolution of CMB temperature. Solid lines show models without PPV while dotted lines are for models with PPV weaker by two orders of magnitude.

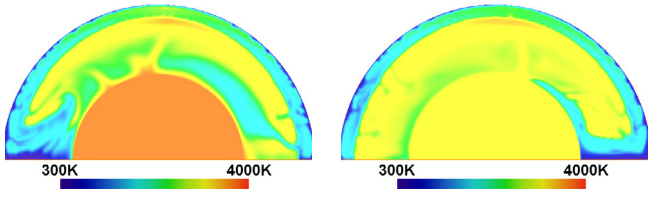

(a) P0-10^8kα4500H2 (b) P2-10^8kα4500H2

Fig. 7. Snapshot of temperature taken at 4.5 Ga for models P-10^8kα4500H2.

enforces partially layered convection. Strong features penetrate the boundary and we thus observe downwellings reaching the CMB. Boundary is however blocking small-scale flow which results in substantial temperature contrast between the upper and lower mantle. PPV first appears in the model after 1 Ga evolution from the initial state in sporadic isolated patches (Fig. 8a) – earlier than in a corresponding model with lower $Ra = 10^7$. These patches are caused by an avalanche of cold upper mantle material penetrating 660 km boundary and arriving at the CMB. Presence of weak PPV is reflected in increased CMB heat flux (Fig. 8b) and somewhat enhanced core cooling (Fig. 8d). PPV then temporarily disappears and until 2.5 Ga plays hardly any role. At 2.5 Ga next massive ava-

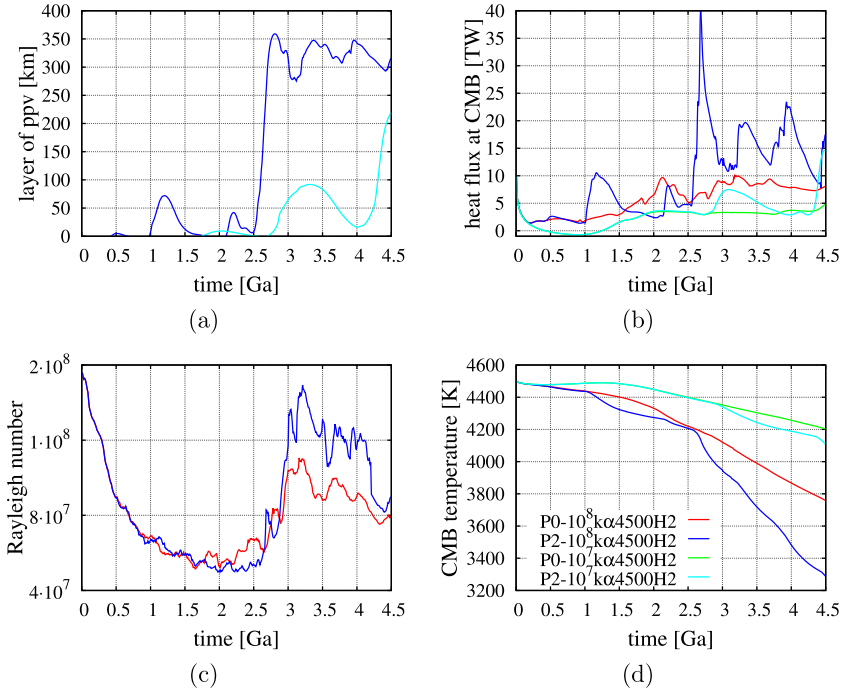

Fig. 8. Models P-10^8kα4500H2 and P-10^7kα4500H2: time evolution of selected quantities.

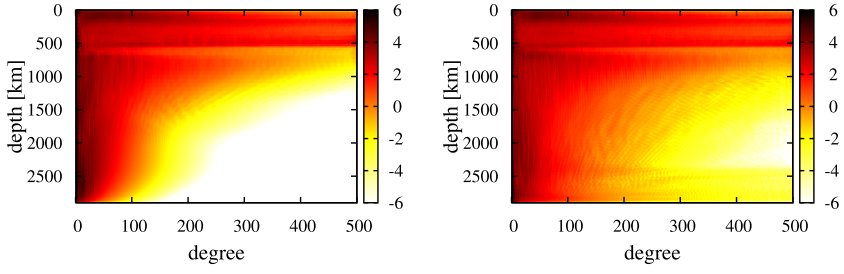

Fig. 9. Models P-10^8kα4500H2: power spectrum of temperature anomalies averaged over last 0.5 Ga of the model runs. Left panel is for model without PPV, right panel is for model with PPV.

lanche of cold material cools lowermost mantle and since that moment PPV lenses are present as indicated in Fig. 8a, where average PPV thickness is plotted as a function of time. Since then CMB heat flux is strongly enhanced (Fig. 8b) and core cooling is much more efficient (Fig. 8d). Final core temperature is thus by more than 400 K lower than in case without weak PPV and average mantle temperature is by about 70 K higher. That is also reflected in horizontally-averaged viscosity profile (Fig. 4b)—model with weak PPV results in considerably weaker lower mantle. Time evolution of *Ra* in models P-10^8kα4500H2, with and without PPV is shown in Fig. 8c. *Ra* is first decreasing (up to ∼2 Ga), thus reflecting cooling of the upper mantle in the initial period when the upper and the lower mantle convective systems are almost isolated by 660 km endothermic phase boundary. At about 2.5 Ga these convective systems are connected by a massive avalanche event. This avalanche decreases lower mantle temperature and in turn increases upper mantle temperature. The viscosity at 500 km thus decreases considerably through thermal effect and we observe steep increase of *Ra* with time. This effect is stronger in the model with weak PPV (blue line), where lower mantle was warmer. Besides the effect of 660 km phase transition the volumetric heating may play a role here similarly to previously discussed case P0-$10^7$4300H1. At a time of ∼ 2 Ga internal heating becomes lower than 35 TW and plume activity is increasing. Enhanced mobility of the lowermost mantle is further reflected in shift of the spectra of temperature anomalies (Fig. 9). As shown by (Nakagawa and Tackley, 2004b), presence of regular PPV (with the same viscosity as that of perovskite) produces upwellings with smaller horizontal scale than observed in models without PPV. Here we demonstrate that this effect of an exothermic transition is enhanced by the low viscosity of PPV. In the model without PPV cold material arriving at the CMB is stiff and forms large scale anomalies in the lowermost mantle (Fig. 9a). If weak PPV is assumed, cold material at the base of the downwellings can easily spread horizontally and enhanced lateral flow in the lowermost mantle then results in significantly smaller scale features (Fig. 9b).

4. Conclusions

The effects of variable material properties (thermal expansivity, diffusivity) on mantle convection were already discussed in numerous studies. Decreasing expansivity and increasing diffusivity both suppress convective vigour in the deep mantle and result in larger scale structures. Increase of thermal conductivity in the lower mantle supports generation of broad lower mantle plumes (e.g. Matyska et al., 1994; Dubuffet et al., 2002) and increases man-

tle temperature (van den Berg and Yuen, 2002; Monnereau and Yuen, 2010). Van den Berg et al. (2005) studied effects of thermal conductivity on mantle thermal evolution and concentrated on contributions from both phonon and radiative components of conductivity (Hofmeister, 1999). They report that temperature and pressure dependent phonon conductivity delays cooling thanks to relatively low conductivity at shallow depths, while radiative contribution that increases lowermost mantle conductivity supports heat extraction from the core and enhances cooling. Here we also observe that including depth-dependent conductivity and expansivity in the models without weak PPV increases average mantle temperature and delays secular cooling through formation of less conductive layer in the uppermost mantle and through less vigorous flow in the lower mantle. Weak PPV has only mild effects on the average mantle temperature, it however significantly affects resulting core temperature and heat flux.

Another important factor that affects secular cooling is initial core temperature. Here we evaluated models with core temperatures ranging between 4,300 K and 6,000 K. Our results show that higher initial core temperatures result in warmer final state of the core. In models with higher initial core temperatures cooling is more efficient and the core temperature drop over the calculation is twice higher in case of $T_{cmb}^{ini} = 6,000$ K than in case with $T_{cmb}^{ini} = 4,300$ K, but the final core temperatures still differ by $\sim 1,200$ K. That is in contradiction with the findings of (Nakagawa and Tackley, 2010), who conclude that in a thermo-chemical model of secular cooling the final state is only weakly dependent on initial CMB temperature unless global high-density layer of subducted MORB material is present. That discrepancy may be attributed to differences between our model setup and model of Nakagawa and Tackley (2010)—among them probably the initial temperature distribution (overheated mantle versus adiabatic structure with potential temperature of 1,650 K) and the rheological description (pressure and temperature dependent viscosity with mild contrasts versus pressure and temperature dependent viscosity with plastic yielding mobilising the lithosphere) play the important role. Furthermore, our model does not take into account heat transfer due to partial melting that may be crucial for heat transfer by mantle convection (Nakagawa et al., 2012b). Our results are on the other hand in agreement with the cooling models of van den Berg et al. (2005), who also report that the final state depends on initial CMB temperature. Final CMB temperature in our models with variable parameters falls into range 3,400–5,300 K. The recent estimate of the CMB temperature based on melting temperature of iron at the inner core boundary (Anzellini et al., 2013) is $4,050 \pm 500$ K. On the other hand, based on the measurements of solidus temperature of pyrolitic mantle Nomura et al. (2014) argue that the upper bound of T_{cmb} is $3,570 \pm 200$ K. Combining these evidences, we could conclude that the results of our models with higher Ra that yield relatively low final CMB temperature are consistent with these estimates and model with the weak PPV is close to the lower bound of the CMB temperature estimate. As a consequence, PPV is present not only in the cold downwellings, but in wider regions of the lowermost mantle.

In agreement with previous studies (e.g. Nakagawa and Tackley, 2011) we show that weak post-perovskite in the bottom thermal boundary layer tends to destabilize flow and enhance convective vigour. The effects of weak post-perovskite on the average mantle temperature are rather small. The resulting core temperature on the other hand is by 180 K lower if post-perovskite weaker by two orders of magnitude is considered and by 260 K lower if the post-perovskite viscosity is reduced by a factor of 1000 in the models with constant parameters. The effect is probably even more pronounced with yet weaker PPV. When variable mantle parameters and higher Ra are assumed, core temperature may be by more than 400 K lower if PPV weaker by two orders of magnitude is taken into account. Weak PPV further enhances CMB heat flux (Nakagawa and Tackley, 2011; Čížková et al., 2010; Li et al., 2014). Heat flux variations with time reflect episodes of massive cold downwellings arriving at the CMB associated with post-perovskite formation. Such episodic heat flux variations may be required to induce changes in geodynamo reversal behaviour (Biggin et al., 2012). Detailed discussion of magnetic field evolution is however beyond the scope of this paper, as inner core growth and magnetic dissipation are not considered in our models.

Presented model is certainly oversimplified in several aspects. Among them axisymmetric 2D approximation of a 3D process, absence of compositional heterogeneity in the lowermost mantle or rheology yielding mobile-lid instead of plate tectonics are perhaps most limiting. It can therefore not provide complex and fully realistic description of the cooling process. Our results on the other hand demonstrate that rheologically weak PPV significantly enhances core cooling and its effect on core temperature is opposite and comparable in amplitude with the effects of other key parameters such as thermal conductivity or expansivity.

Acknowledgements

We thank Arie van den Berg, Ondřej Čadek and Ctirad Matyska for fruitful discussions and Frédéric Deschamps and Takashi Nakagawa, for constructive reviews that significantly improved the manuscript.

References

Amit, H., Choblet, G., 2009. Mantle-driven geodynamo features-effects of post-perovskite phase transition. Earth, Planets Space 61 (11), 1255–1268.
Ammann, M.W., Brodholt, J.P., Wookey, J., Dobson, D.P., 2010. First-principles constraints on diffusion in lower-mantle minerals and a weak D″ layer. Nature 465 (7297), 462–465.
Anzellini, S., Dewaele, A., Mezouar, M., Loubeyre, P., Morard, G., 2013. Melting of iron at Earth's inner core boundary based on fast X-ray diffraction. Science 340 (6131), 464–466.
Benešová, N., Čížková, H., 2012. Geoid and topography of Venus in various thermal convection models. Stud. Geophys. Geod. 56 (2), 621–639.
Biggin, A.J., Steinberger, B., Aubert, J., Suttie, N., Holme, R., Torsvik, T.H., van der Meer, D.G., van Hinsbergen, D.J.J., 2012. Possible links between long-term geomagnetic variations and whole-mantle convection processes. Nature Geosci. 5 (9), 674.
Breuer, D., Spohn, T., 1993. Cooling of the Earth, Urey ratios, and the problem of potassium in the core. Geophys. Res. Lett. 20 (15), 1655–1658.
Butler, S.L., Peltier, W.R., 2002. Thermal evolution of Earth: models with time-dependent layering of mantle convection which satisfy the Urey ratio constraint. Geophys. Res. Solid Earth 107 (B6), ESE 3-1–ESE 3-15.
Čadek, O., Fleitout, L., 2006. Effect of lateral viscosity variations in the core–mantle boundary region on predictions of the long-wavelength geoid. Stud. Geophys. Geod. 50, 217–232.
Carrez, P., Ferr, D., Cordier, P., 2007. Peierls-Nabarro model for dislocations in $MgSiO_3$ post-perovskite calculated at 120 GPa from first principles. Philos. Mag. 87 (22), 3229–3247.
Catalli, K., Shim, S.-H., Prakapenka, V., 2009. Thickness and Clapeyron slope of the post-perovskite boundary. Nature 462 (7274), 782–785.
Čížková, H., Čadek, O., Matyska, C., Yuen, D.A., 2010. Implications of post-perovskite transport properties for core–mantle dynamics. Phys. Earth Planet. Inter. 180, 235–243.
DeLandro-Clarke, W., Jarvis, G.T., 1997. Numerical models of mantle convection with secular cooling. Geophys. J. Int. 129 (1), 183–193.
Deschamps, F., Tackley, P.J., Nakagawa, T., 2010. Temperature and heat flux scalings for isoviscous thermal convection in spherical geometry. Geophys. J. Int. 182 (1), 137–154.
Dubuffet, F., Yuen, D.A., Rainey, E.S.G., 2002. Controlling thermal chaos in the mantle by positive feedback from radiative thermal conductivity. Nonlinear Processes Geophys. 9 (3/4), 311–323.
Hofmeister, A.M., 1999. Mantle values of thermal conductivity and the geotherm from phonon lifetimes. Science 283 (5408), 1699–1706.
Honda, S., Iwase, Y., 1996. Comparison of the dynamic and parameterized models of mantle convection including core cooling. Earth Planet. Sci. Lett. 139 (12), 133–145.
Karato, S., 2010. The influence of anisotropic diffusion on the high-temperature creep of a polycrystalline aggregate. Phys. Earth Planet. Inter. 183 (34), 468–472.

Karato, S., Riedel, M.R., Yuen, D.A., 2001. Rheological structure and deformation of subducted slabs in the mantle transition zone: implications for mantle circulation and deep earthquakes. Phys. Earth Planet. Inter. 127 (14), 83–108.
Korenaga, J., 2006. Archean geodynamics and the thermal evolution of earth. In: Benn, J.-C.M.K., Condie, K. (Eds.), Archean Geodynamics and Environments. AGU, pp. 7–32.
Korenaga, J., 2010. Scaling of plate tectonic convection with pseudoplastic rheology. J. Geophys. Res. Solid Earth 115 (B11).
Labrosse, S., Jaupart, C., 2007. Thermal evolution of the Earth: secular changes and fluctuations of plate characteristics. Earth Planet. Sci. Lett. 260 (34), 465–481.
Li, Y., Deschamps, F., Tackley, P.J., 2014. Effects of low-viscosity post-perovskite on the stability and structure of primordial reservoirs in the lower mantle. Geophys. Res. Lett. 41 (20), 7089–7097. http://dx.doi.org/10.1002/2014GL061362, ISSN 1944-8007.
Lowrie, W., 2007. Fundamentals of Geophysics. Cambridge University Press.
Matyska, C., Yuen, D.A., 2005. The importance of radiative heat transfer on superplumes in the lower mantle with the new post-perovskite phase change. Earth Planet. Sci. Lett. 234 (12), 71–81.
Matyska, C., Yuen, D.A., 2006. Lower mantle dynamics with the post-perovskite phase change, radiative thermal conductivity, temperature- and depth-dependent viscosity. Phys. Earth Planet. Inter. 154 (2), 196–207.
Matyska, C., Moser, J., Yuen, D.A., 1994. The potential influence of radiative heat transfer on the formation of megaplumes in the lower mantle. Earth Planet. Sci. Lett. 125 (14), 255–266.
Matyska, C., Yuen, D.A., Wentzcovitch, R.M., Čížková, H., 2011. The impact of variability in the rheological activation parameters on lower-mantle viscosity stratification and its dynamics. Phys. Earth Planet. Inter. 188 (12), 1–8.
Monnereau, M., Yuen, D.A., 2007. Topology of the postperovskite phase transition and mantle dynamics. P. Natl. Acad. Sci. USA 104 (22), 9156–9161.
Monnereau, M., Yuen, D.A., 2010. Seismic imaging of the D″ and constraints on the core heat flux. Phys. Earth Planet. Inter. 180 (34), 258–270.
Murakami, M., Hirose, K., Kawamura, K., Sata, N., Ohishi, Y., 2004. Post-perovskite phase transition in $MgSiO_3$. Science 304 (5672), 855–858.
Nakagawa, T., Tackley, P.J., 2004a. Effects of thermo-chemical mantle convection on the thermal evolution of the Earths core. Earth Planet. Sci. Lett. 220 (12), 107–119.
Nakagawa, T., Tackley, P.J., 2004b. Effects of a perovskite-postperovskite phase change near core–mantle boundary in compressible mantle convection. Geophys. Res. Lett. 31 (16).
Nakagawa, T., Tackley, P.J., 2005a. Deep mantle heat flow and thermal evolution of the Earth's core in thermochemical multiphase models of mantle convection. Geochem. Geophys. Geosyst. 6 (8).
Nakagawa, T., Tackley, P.J., 2005b. The interaction between the post-perovskite phase change and a thermo-chemical boundary layer near the core–mantle boundary. Earth Planet. Sci. Lett. 238 (12), 204–216.
Nakagawa, T., Tackley, P.J., 2006. Three-dimensional structures and dynamics in the deep mantle: effects of post-perovskite phase change and deep mantle layering. Geophys. Res. Lett. 33 (12).
Nakagawa, T., Tackley, P.J., 2008. Lateral variations in CMB heat flux and deep mantle seismic velocity caused by a thermal–chemical-phase boundary layer in 3D spherical convection. Earth. Planet. Sc. Lett. 271 (1–4), 348–358.
Nakagawa, T., Tackley, P.J., 2010. Influence of initial CMB temperature and other parameters on the thermal evolution of Earth's core resulting from thermochemical spherical mantle convection. Geochem. Geophys. Geosyst. 11, Q06001.
Nakagawa, T., Tackley, P.J., 2011. Effects of low-viscosity post-perovskite on thermo-chemical mantle convection in a 3-D spherical shell. Geophys. Res. Lett. 38, L04309.
Nakagawa, T., Tackley, P.J., 2012a. Three-dimensional structures and dynamics in the deep mantle: Effects of post-perovskite phase change and deep mantle layering. Geophys. Res. Lett. 33, L12S11.
Nakagawa, T., Tackley, P.J., 2012b. Influence of magmatism on mantle cooling, surface heat flow and Urey ratio. Earth Planet. Sci. Lett. 329330, 1–10.
Nomura, R., Hirose, K., Uesugi, K., Ohishi, Y., Tsuchiyama, A., Miyake, A., Ueno, Y., 2014. Low core–mantle boundary temperature inferred from the solidus of Pyrolite. Science 343 (6170), 522–525.
Oganov, A.R., Ono, S., 2004. Theoretical and experimental evidence for a post-perovskite phase of $MgSiO_3$ in Earth's D″ layer. Nature 430, 445–448.
Samuel, H., Tosi, N., 2012. The influence of post-perovskite strength on the Earth's mantle thermal and chemical evolution. Earth. Planet. Sc. Lett. 323–324 (0), 50–59.
Solomatov, V.S., Moresi, L.-N., 2002. Small-scale convection in the D″ layer. J. Geophys. Res. Solid Earth 107 (B1), ETG 3-1–ETG 3-10.
Sotin, C., Labrosse, S., 1999. Three-dimensional thermal convection in an iso-viscous, infinite Prandtl number fluid heated from within and from below: applications to the transfer of heat through planetary mantles. Phys. Earth Planet. Inter. 112 (34), 171–190.
Tateno, S., Hirose, K., Sata, N., Ohishi, Y., 2009. Determination of post-perovskite phase transition boundary up to 4,400 K and implications for thermal structure in D″ layer. Earth. Planet. Sc. Lett. 277 (1–2), 130–136.
Tosi, N., Čadek, O., Martinec, Z., Yuen, D.A., Kaufmann, G., 2009. Is the long-wavelength geoid sensitive to the presence of postperovskite above the core–mantle boundary? Geophys. Res. Lett. 36 (5).
Tosi, N., Yuen, D.A., Čadek, O., 2010. Dynamical consequences in the lower mantle with the post-perovskite phase change and strongly depth-dependent thermodynamic and transport properties. Earth. Planet. Sc. Lett. 298 (1–2), 229–243.
Travis, B., Olson, P., 1994. Convection with internal heat sources and thermal turbulence in the Earth's mantle. Geophys. J. Int. 118 (1), 1–19.
Tsuchiya, T., Tsuchiya, J., Umemoto, K., Wentzcovitch, R.M., 2004. Phase transition in $MgSiO_3$ perovskite in the Earth's lower mantle. Earth Planet. Sci. Lett. 224 (3-4), 241–248.
van den Berg, A.P., Yuen, D.A., 2002. Delayed cooling of the Earths mantle due to variable thermal conductivity and the formation of a low conductivity zone. Earth Planet. Sci. Lett. 199 (34), 403–413.
van den Berg, A., Yuen, D., Rainey, E., 2004. The influence of variable viscosity on delayed cooling due to variable thermal conductivity. Phys. Earth Planet. Inter. 142 (34), 283–295.
van den Berg, A.P., Rainey, E.G., Yuen, D., 2005. The combined influences of variable thermal conductivity, temperature- and pressure-dependent viscosity and coremantle coupling on thermal evolution. Phys. Earth Planet. Inter. 149 (34), 259–278.
van den Berg, A.P., Hoop, M.V.D., Yuen, D.A., Duchkov, A., van der Hilst, R.D., Jacobs, M.H., 2010. Geodynamical modeling and multiscale seismic expression of thermo-chemical heterogeneity and phase transitions in the lowermost mantle. Phys. Earth Planet. Inter. 180 (34), 244–257.
van Hunen, J., van den Berg, A.P., Vlaar, N.J., 2004. Various mechanisms to induce present-day shallow flat subduction and implications for the younger Earth: a numerical parameter study. Phys. Earth Planet. Inter. 146 (12), 179–194.
van Schmus, W.R., 1995. Natural radioactivity of the crust and mantle. In: Ahrens, T. J. (Ed.), Global Earth Physics: A Handbook of Physical Constants. AGU, pp. 283–291.